High-pressure melting curves of alkali halides

Reinhard Boehler
Max-Planck-Institute fur Chemie, Postfach 3060, 55020 Mainz, Germany

Marvin Ross and David B. Boercker
Lawrence Livermore National Laboratory, University of California, Livermore, California 94551
(Received 12 May 1995)

The melting curves of CsI, KCl, and KBr were measured in a diamond-anvil cell to temperatures of 3500 K and pressures up to 370 kbar. Theoretical calculations for CsI, made by directly integrating the Clapeyron equation, are in good agreement with the measurements and predict a crossing of the CsI and Xe melting curves near 410 kbar and 4280 K.

I. INTRODUCTION

Of the known first-order phase transitions, melting covers the widest range of pressures and temperatures. Consequently, melting data provides a potentially rich source of information regarding the role played by interatomic forces in determining pressure and temperature-induced changes in solids and liquids. Recent advances, particularly the development of high-temperature diamond-anvil cell techniques, have led to an order of magnitude increase in the pressure range accessible for study.[1] Much of this effort has been motivated by a need for melting data of oxides and silicates for the purpose of understanding the structure and dynamics of the Earth's interior. These systems are mixtures of ions for which the interatomic forces are the sum of a long-range Coulomb interaction and a short-range potential which is often covalent and directional. As a result the melting curves of such systems have proven difficult to predict reliably. In the case of the rare-gas solids, the interatomic forces are short-ranged and nondirectional, or spherical. For these systems theoretical calculations have been made and measurements of melting curves have played an important role in validating their accuracy and for judging the usefulness of simpler models. One step up in complexity from the rare-gases are alkali halides, which are the subject of this paper. These are binary systems which combine long-ranged Coulomb forces with the same type of short-range potentials characteristic of inert gas atoms. Despite their relative simplicity, the complication of both long-range and short-range potentials have left the theory of alkali-halide melting in poor shape.

In Sec. II of this paper we report measurements of the melting curves of CsI, KCl, and KBr to temperatures up to 3500 K and pressures to 370 kbar. These are the highest temperature melting data measured statically for an alkali halide and extend the pressure range by more than an order of magnitude over previous measurements. Calculations of the melting curve were made for CsI by a direct integration of the Clausius-Clapeyron equation and are reported in Sec. III. Section IV presents the calculation of a xenon melting curve with a comparison to CsI. The results of the paper are discussed in Sec. V.

A reason for choosing CsI as the object of the present calculations was to examine the possible convergence of the melting curves of CsI and Xe at very high pressure. These materials are isoelectronic. Cs^+ and I^- both have Xe-like closed-shell electronic configurations. At 1 bar pressure the stable structures of CsI and Xe are, respectively, the CsCl and fcc structures. However with increasing density it is the strong repulsive forces between the Cs^+ and I^- ion cores that mainly determine the pressure and crystal structure. As a result solid Xe and CsI have virtually identical isotherms above 10 kbar,[2] and both are found to transform to hcp or hcp-like structures. Xe transforms continuously from fcc to hcp over the pressure range 75 to 140 kbar (Ref. 3) and CsI, which is initially in a CsCl structure, begins its transformation at 400 kbar. Both materials also undergo metallization transitions by band overlap at comparable pressures. CsI metallizes near 1.1 Mbar (Ref. 4) and Xe near 1.32 Mbar.[4,5] Since both materials are isoelectronic and have very similar properties at high pressure we decided to investigate the possibility that the melting curves of the two might also converge. The melting curve of Xe was obtained by corresponding states theory and compared with CsI.

Recently, it was brought to our attention that Kofke[6,7] had used the method of Clapeyron integration to calculate phase coexistence along the liquid-vapor saturation line. Although Kofke's particular numerical method is more appropriate to the compressible system he studied, his reported experience and insight were very helpful.

II. EXPERIMENT

The melting experiments were carried out in a laser-heated diamond-anvil cell. The alkali halides of pure quality (99.999%) were loaded in the pressure cell (see Fig. 1) together with a strip of flattened tungsten wire and several ruby chips. Prior to pressurizing, the high-pressure cell was dried in a vacuum at 120 °C and subsequently flushed with dry argon. Pressures and pressure gradients were measured using the ruby scale. The tungsten strip was heated with a 25 W yttrium-lithium-fluoride (YLF) laser ($\lambda = 1.05$ μm). Below the melting temperature samples neither absorb this radiation nor emit incandescent light. The defocused laser beam created a hot spot on the tungsten strip of about 20–30 μm in diameter. Temperatures were measured from the central region of this hot spot from an area with 1 μm in diameter in

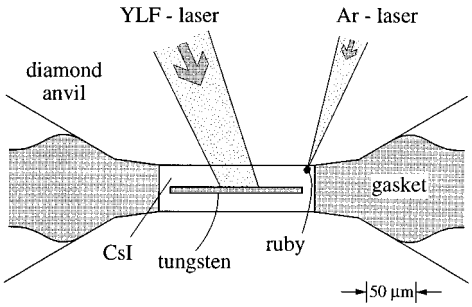

FIG. 1. Schematic cross section through a diamond-anvil cell assembly.

the special range 550–800 nm using a CCD (charge coupled device)-detector technique and by fitting the emission spectra to a Planck radiation function. Details of this measurement are described elsewhere.[8] When the surface temperature of the tungsten strip reached the melting temperature of the sample, a large increase in temperature was observed due to a strong increase in the absorption (and emission) of the sample. The nature of this change in absorption is unknown. The melting temperatures were measured by slowly increasing the laser power while recording temperatures in rapid sequence, and the melting temperatures reported here are the last recording before the large discontinuous change in temperature. The reproducibility of this method in most cases was within 100 K except for the highest pressures of this study where the solid-liquid transition was less sharp due to an increase in absorption of the solid. The surface of the tungsten strip did not show any sign of chemical reaction subsequent to melting.

Figure 2 shows the melting measurements for CsI, KBr, and KCl. The data are in Table I. The average errors bars are

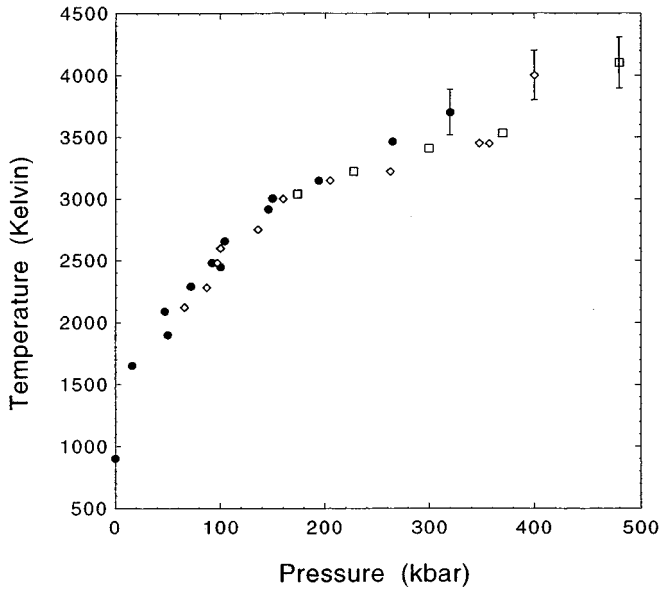

FIG. 2. Melting curves of CsI (●), KBr (◇), and KCl (□) plotted as temperature versus pressure. Included are the measured shock melting points of these compounds as indicated by the same symbols with a bar.

TABLE I. Melting temperatures of CsI, KBr, and KCl at high pressures.

P (kbar)	T_m (K)
CsI	
0	899
16	1653±13
47	2090±30
50	1900±50
72	2290±30
92	2483±3
104	2660±76
146	2917±3
150	3085±15
194	3150±65
265	3466±134
KBr	
0	1007
66	2120±20
87	2280±20
97	2480±20
100	2600±50
136	2570±50
160	3000±50
205	3149±39
263	3220±50
348	3450±60
357	3447±73
KCl	
0	1043
174	3040±40
228	3220±80
300	3410±50
370	3540±90

about 3 kbar in pressure and 45 K in temperature. They are due mainly to uncertainties in the pressure gradients and the thermal pressure and represent the temperature variation of at least five different measurements of melting using the method described above. A striking feature of the data in Fig. 2 is the similarity of the three curves. This suggests that all the materials undergo the same pressure-induced changes.

Our melting data on KCl and KBr are in excellent agreement with those measured by Pistorious[9] in a piston-cylinder apparatus to 41 kbar. There are no previous static melting data of CsI at high pressure. Also plotted in Fig. 2 are melting points of these three compounds that were reported by researchers using shock wave techniques.[10–12] These data tend to be at temperatures slightly higher than ours. We believe that this discrepancy is consistent with the recent observations of Boness and Brown[13] that melting of KCl and KBr on the Hugoniot exhibits superheating ''of several hundred Kelvin.'' The overall agreement of the present diamond-anvil measurements with both precise low-pressure measurements and those of shock wave experiments confirms the

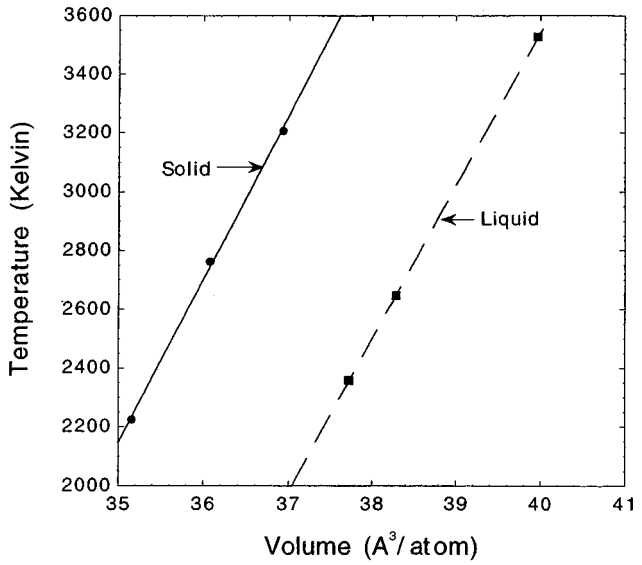

FIG. 3. Temperature (K) versus volume (Å^3/atom) at 100 kbar calculated for solid and liquid CsI.

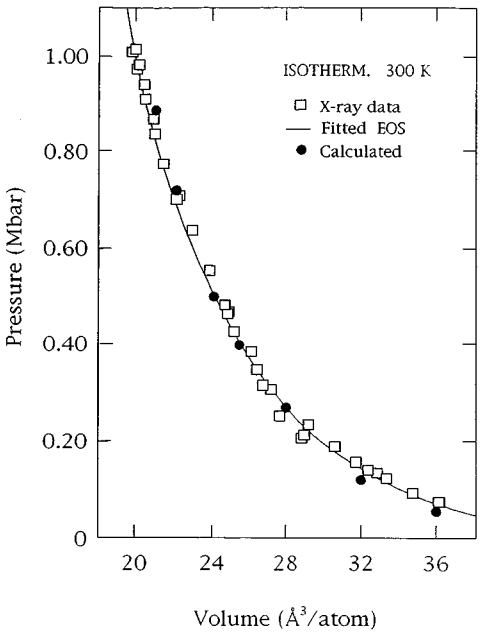

FIG. 4. Pressure-volume CsI solid isotherm at 300 K. Black circles are calculated by molecular dynamics in this paper. Squares are x-ray data and solid curve is a fit to x-ray data (Ref. 3).

reliability of this relatively new advance, at least for this class of materials.

III. THEORETICAL

A. Thermodynamic integration of the Clapeyron equation

In this section we present a computer simulation method to determine the melting curve of a solid. The two fundamental expressions that govern phase equilibria are the equality of the Gibbs free energy of the coexisting phases and the Clausius-Clapeyron equation. For any two phases in equilibrium the temperature, pressure, and Gibbs free energies must be equal:

$$G(T,P)_l = G(T,P)_s . \tag{1}$$

The Clausius-Clapeyron equation follows directly from the Gibbs equality[14] and is written as

$$dT/dP = (T\Delta V/\Delta H), \tag{2}$$

where ΔV and ΔH are, respectively, the difference in molar volume $(V_l - V_s)$ and enthalpy $(H_l - H_s)$ of the coexisting phases. The equation does not determine the location of the melt line but it predicts the slope of the line separating the coexisting phases starting from a known reference point. In this paper we chose the reference as the 1 bar melting point and integrate the Clapeyron equation to obtain the full melting curve.

The enthalpy and volume of the coexisting phases were calculated at a series of temperatures and pressures using a constant pressure molecular-dynamics simulation program. After completing a sizable number of calculations it became apparent that the ratio $(\Delta V/\Delta H)$ is almost independent of temperature, at constant pressure, over the pressure range of our interest. The reason is that dense fluids and solids have very similar thermal expansions and heat capacities. As a result at constant pressure, changes in volume or energy with temperature of the coexisting phases are in the same direction and largely cancel. This is illustrated in Fig. 3 which shows the calculated solid and liquid volumes versus temperature at 100 kbar. Since the Clapeyron equation considers only the ratio $\Delta V/\Delta H$, changes in ΔV and ΔH with temperature will be in the same direction and partially canceled. Therefore at fixed pressure, $\Delta V/\Delta H$ can be considered independent of temperature and the Clapeyron equation can be integrated as

$$\ln(T/T_0) = \int (\Delta V/\Delta H) dP. \tag{3}$$

Integration requires a reference melting pressure (P_0) and temperature (T_0) which are chosen as the experimental values for CsI at 1 bar and 903 K. Any inconsistency between the predicted melting temperature and the one at which $\Delta V/\Delta H$ was calculated is easily corrected by an iterative procedure. The nice features of Clapeyron integration is that it avoids a direct determination of free energies and requires only differences in volume and enthalpy which are easily and accurately computed by constant pressure molecular dynamics.

Other methods used to calculate melting curves using molecular dynamics are direct simulation and free-energy integration. Direct simulation approaches attempt to determine melting by observing the change in ordering of a solid going into the liquid. This method does not insure the presence of a reversible path and transformation typically takes place when the solid becomes mechanically unstable. The actual phase transition is bracketed by a region of hysteresis.[15] This is illustrated in Fig. 3 where the metastable points are in the solid above the melting point at 2670 K and in the liquid below this temperature. Ironically, this feature of metastability in computer simulations simplifies the calculation of $\Delta V/\Delta H$ for integrating the Clapeyron equation.

In order to locate the phase transition precisely one needs accurate free energies of both phases. For the case of simple

systems, such as rare gases and many monatomic metals, theoretical models are available for obtaining accurate thermodynamic data for the liquid and solid.[16] In the case of systems where accurate models are not available a useful approach has been to use a series of simulations to calculate differences of free energy from some idealized state in which the free energy is known exactly. For example, Hoover and Ree[17] obtained the free energy of the hard-sphere and hard disk solids starting from a lattice gas with one atom per lattice cell. The Helmholtz free energy of the solid is then obtained by integrating

$$A_{\text{solid}}(V_1)=A_{\text{lattice gas}}(V_0)-\int P(V)dV, \tag{4}$$

where $P(V)$ is obtained by computer simulation. Hoover *et al.*[18] have also shown that the low-temperature harmonic solid provides a convenient reference system for studying the equation of state of inverse power potentials. Hard-sphere and inverse power potentials have the nice feature that their entire equation of state can be determined by computing a single isotherm expressed in reduced units of the potential parameters. This allows the equation of state to be scaled to arbitrary temperatures. This is not the case for real materials for which many isotherms and melting points are required to determine an equation of state.

The similarity between the Clapeyron and free-energy integration methods becomes apparent when examining the derivation of the Clapeyron equation. Equation (1) determines the state of equilibrium between the two phases in terms of the equality of the Gibbs energy. At a slightly different temperature and pressure the Gibbs free energy of the solid (or liquid) is written as

$$G_s(P_1,T_1)=G_s(P_0,T_0)+V_s dP-S_s dT. \tag{5}$$

Equations (4) and (5) are similar in the sense that the right-hand side of both are written in terms of a reference free energy and a ''correction,'' or perturbation term. By equating the Gibbs free energies of the liquid and solid as in Eq. (1), the $G(P_0,T_0)$ terms cancel and the correction terms leads to the Clapeyron equation which give the changes in the melting curve. The reference properties we use for the Clapeyron equation are P_0 and T_0.

B. Intermolecular potential

The intermolecular potential for CsI was the same as that employed in a previous high-pressure study.[19] The assumption is made that the interaction between the ions can be approximated by a xenon-like exponential-six pair potential between closed-shell cores plus a Coulomb interaction between the charges. The justification for this approximation comes from the fact that CsI and xenon have virtually identical isotherms above 10 kbar and should have the same repulsion at small interatomic separations. Therefore we write

$$\phi(r_{ij})=Z_iZ_je^2/r_{ij}+\phi_{\text{exp6}}(r_{ij}), \tag{6}$$

where

$$\phi_{\text{exp6}}(r_{ij})=\varepsilon[6/(\alpha-6)\exp\{\alpha(1-r/r^*)\}-\alpha/(\alpha-6)(r^*/r)^6]. \tag{7}$$

The parameters in Eq. (7) are $\alpha=13$, $r^*=4.47$ A, and $\varepsilon/k=235$ K, where k is the Boltzmann constant. Figure 4 shows a comparison of the calculated room temperature CsI solid isotherm with the x-ray data of Mao *et al.*[3] The excellent agreement at the higher pressures reflects the bias of the present potential to optimize the fit to high-pressure high-temperature data. This led to some difficulty in determining the correct low-pressure value of $(\Delta V/\Delta H)$. Although this potential predicts correctly that CsCl is the stable structure at room temperature it predicts incorrectly that the solid melts from a NaCl structure at 20 kbar and below. In addition since the CsI liquid at $P=0$ is 28.5% expanded from the solid, accurate calculations of the liquid volume and enthalpy are not possible. The failure to correctly predict the structure at melting appears to result from the approximation in using the same core-core repulsion for both ions or in effect assuming both are the same size. It is known that although CsI, CsBr, and CsCl are the only alkali halides to crystallize in a CsCl lattice at room temperature and 1 bar, only CsCl undergoes a transition to a NaCl structure prior to melting. Of the three solids, it is the Cs^+ and Cl^- ions which have most nearly the same sized ions. The ratio of ionic radii R_{Cs^+}/R_{Cl^-} being 0.93 as compared to 0.78 for R_{Cs^+}/R_{I^-}.

The value of $\Delta V/\Delta H$ below 20 kbar was obtained by two methods: (1) calculations made using the CsI potential of Dixon and Sangster[20] and (2) fitting the experimental data. The Dixon-Sangster potential employs a Tosi-Fumi-type function which was fitted to low-pressure data but does not correctly predict the high-pressure equation of state. Therefore the value of $\Delta V/\Delta H$ at 20 kbar was adjusted to ensure a smooth fit between the calculations made at higher pressure and lower pressure. The final value of $\Delta V/\Delta H$ was an average of the two and corresponded to an adjustments of about 5% in each. In the alternative procedure the 1 bar value of $(\Delta V/\Delta H)$ was obtained by a fit to the experimental data. But making accurate low-pressure measurements or calculations is made difficult by the steepness of the melt curve below 20 kbar, so a precise value of $\Delta V/\Delta H$ at $P=1$ bar is uncertain. Nevertheless, both methods for determining the low-pressure slope gave predictions of the melting curve that differ in temperature only by 2%.

C. Molecular-dynamics simulations

The values of H and V in the solid and liquid were obtained by constant pressure molecular dynamics with variable cell shape. In its simplest form molecular-dynamics simulates atomic-scale phenomena by solving Newton's equations of motion of the trajectories of many particles contained in a periodically reproduced computational cell. If a solid phase is being simulated, the number of particles in the cell must be commensurate with the translational symmetry of the crystal. Recently, Parrinello and Rahman[21] introduced a technique in which the size and shape of the computational cell can be allowed to vary in such a way as to keep the pressure fixed at a predetermined value. This method is very effective for studying the stability of solid structures, since the system can spontaneously transform from one crystal type to another through deformation of the computational cell. Implementation of this method for the short-range potential is by now standard[22] and has been employed previ-

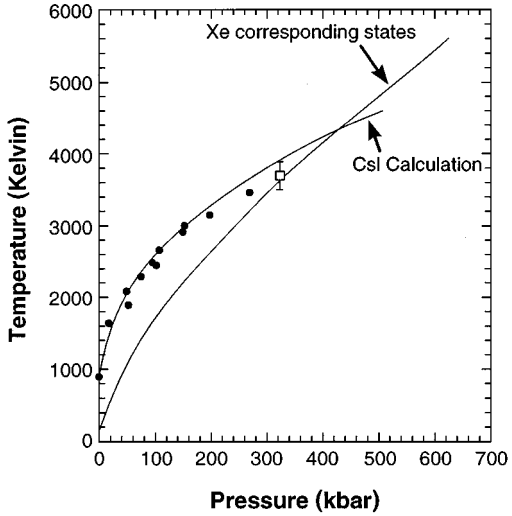

FIG. 5. Melting curves of CsI and Xe. Diamond-anvil measurements of CsI (●) and calculations for CsI from integration of Clapeyron equation. The CsI shock melting point is indicated by the bar. The Xe melting curve was obtained by corresponding states theory as described in text.

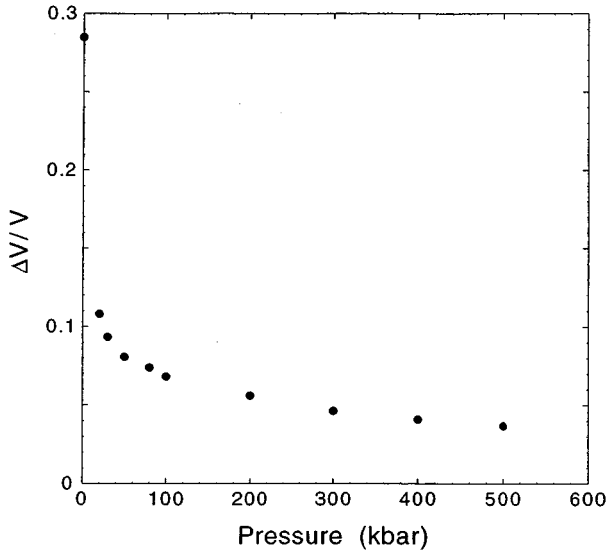

FIG. 6. $\Delta V/V$, volume fraction change on melting for CsI, plotted against the melting pressure.

ously by one of us.[23] However, the long-range Coulomb part of the potential used here requires that the algorithm for the Ewald sum be generalized to arbitrary geometry.[24] We have done this, and the results presented here account for this additional feature. All the simulations were made with 108 ions (54 Cs^+ and 54 I^-) in a CsCl supercell, made up of $27(3\times3\times3)$ unit cells of four ions in each. Runs were typically made for 200 to 300 ps with a time step of 10^{-15} sec. The liquid state was generated by restarting a completed solid run with $Z_{i,j}$ set to 0. This destabilized the lattice forming a fluid after which the Z's were reset and the ionic liquid phase was run to equilibrium.

The calculated and measured CsI melting curves are shown in Fig. 5. Also shown is the melting point determined from shock experiments.[12] These data are in good agreement. Included in the figure is the Xe melting curve predicted in Sec. IV from corresponding states theory.

IV. THE XENON MELTING CURVE

The xenon melting curve has been measured to only 400 K and 7 kbar,[25] but measurements of the melting curve for He,[26] Ne,[27] and Ar (Ref. 16) have been made to about 60 kbar. Theoretical calculations have shown that with accurate models of the liquid and solid, and an exp-6 pair potential [Eq. (7)] with parameters fitted to the solid isotherm, it is possible to predict these experimental results quite well. Calculations have been extended to 3000 K.[16,27] Although comparable calculations have not been made specifically for Xe it is a straightforward procedure to obtain such results by scaling the calculated inert gas melting curves using the rule of corresponding states.

The principle of corresponding states is that all systems having the same functional form of the intermolecular potential and will have the same reduced form of the equation of state.[28] Theoretical studies have shown that the intermolecular potentials for rare-gas solids are well described by an exponential-six potential with a stiffness parameter $\alpha=13.0$–13.2. As a consequence, all the thermodynamic properties of these elements may be scaled from a knowledge of the position (r^*) and depth (ε) of the attractive well. An exception is helium over the range in which quantum effects are significant. Thus, given a set of potential parameters for a given rare gas, its melting curve may be predicted with reasonable accuracy.

The Xe melting curve was obtained by scaling from Ar (or Ne) using the following expressions:

$$P(\mathrm{Xe})=P(\mathrm{Ne})\cdot\varepsilon/r^{*3}(\mathrm{Xe})/[\varepsilon/r^{*3}(\mathrm{Ne})] \tag{8}$$

and temperature,

$$T(\mathrm{Xe})=T(\mathrm{Ne})\cdot\varepsilon/k(\mathrm{Xe})/[\varepsilon/k(\mathrm{Ne})], \tag{9}$$

with the Ar(Ne) potential parameters cited in Refs. 16 and 26 and for Xe we took those used in Eq. (7). The results are plotted in Fig. 5 and show that the Xe and CsI curves are expected to cross near 410 kbar and 4280 K. This is beyond the range of the present experiments.

V. DISCUSSION

The detailed atomistic information provided by computer simulations are a valuable adjunct to experiment. In the present study they provide detailed information regarding the pressure-induced changes of atomic order and the thermodynamics of melting. For example, Figs. 6, 7, and 8 show, respectively, the values of $\Delta V/V$, $\Delta V/\Delta H$, and $\Delta H/Nk$ for CsI calculated as a function of melting pressure. Below 100 kbar the volume change decreases rapidly with increasing pressure, while the enthalpy sharply increases. Both changes lead to the large drop in $\Delta V/\Delta H$ which is responsible for the continuous decrease of the melting slope (i.e., Figs. 2 and 5). These results can be understood in terms of the pressure-induced structural changes of the fluid. Figures 9 and 10(a) show the radial distribution functions of the unlike, $g_{+-}(r)$, and like, $g_{++}(r)$ and $g_{--}(r)$, radial distribution

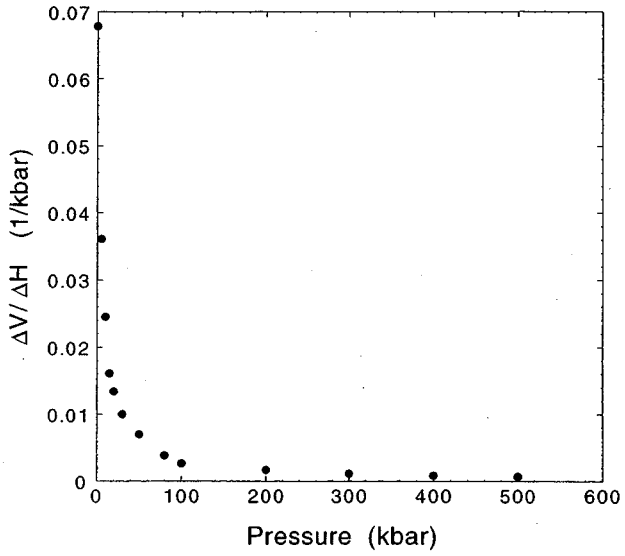

FIG. 7. $\Delta V/\Delta H$ for CsI plotted against the melting pressure.

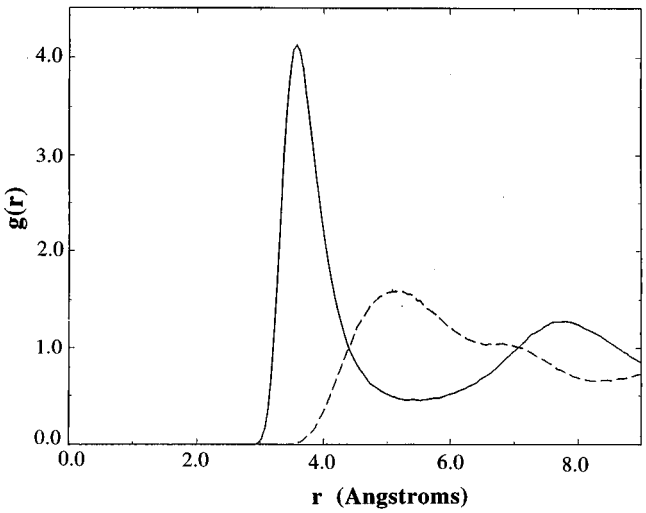

FIG. 9. Radial distribution functions, $g_{+-}(r)$ and $g_{++}(r)$, shown as solid and dashed curves respectively, for fluid CsI calculated near the normal melting point at 0 kbar and 903 K.

functions at 0 and 100 kbar. $g_{+-}(r)$ is related to the probability of finding any positive and negative ion separated by a distance, r. $g_{++}(r)$ and $g_{--}(r)$ are defined similarly for like ions. Note that for the present potential $g_{++}(r) = g_{--}(r)$. Figure 10(b) shows the total radial distribution, $g(r)=[g_{+-}(r)+g_{++}(r)]/2$. $g(r)$ is related to the probability of finding any ion, positive or negative, separated by a distance r.

At 0 kbar the structure is determined by the balance of long-range Coulomb forces and short-range inter-ion core-core repulsions. The action of the Coulomb force is to separate like charges into alternate shells with the result that each liquid atom is surrounded by about five nearest neighbors of opposite charge and a second or next-nearest shell of same charge ions. As the pressure is increased the number of nearest-neighbor ions increases. In the case of CsI evidence for this process is observed even at 1 bar pressure (Fig. 9).

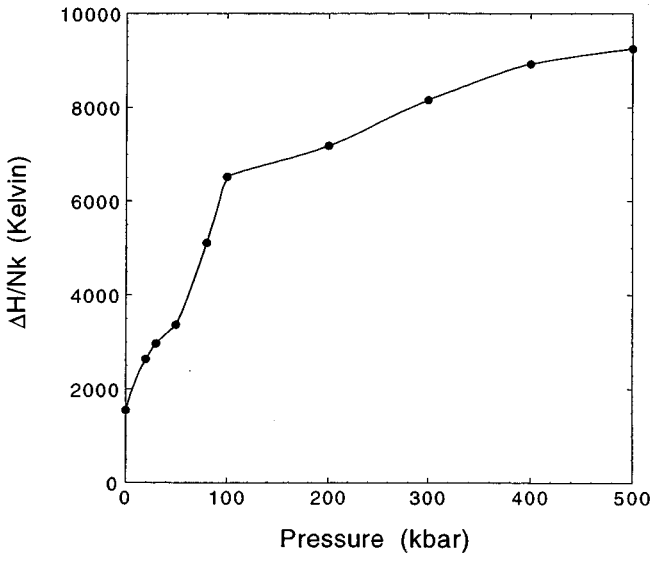

FIG. 8. $\Delta H/Nk$, enthalpy change on melting or CsI plotted against the melting pressure.

There, $g_{++}(r)$ shows a splitting of the second shell in which some same charged ions are closer to the first shell. This splitting grows with increasing pressure with the result that more ions of the same charge in the second shell begin to fill in the first shell. At 100 kbar [Fig. 10(a)] the peak of the second-shell distribution function lies within the envelope of the first shell. At this pressure the repulsive forces between ion cores determine the atomic arrangement which, as shown in Fig. 10(b), is similar to that of an inert gas liquid except that in an alkali halide a charge gradient is present. As a result the changes in the ΔV level off to a relatively constant value at higher pressures and approach values comparable to those found for rare gases. These conclusions were also reached by Ross and Rogers on the basis of hypernetted-chain calculations.[18]

Similarly, changes in the enthalpy mirror those of the volume and liquid structure. At low pressure melting is accompanied by a change from the highly charge-ordered solid arrangement to a less ordered liquid arrangement. Thus melting results in some increase in the Coulomb energy. As the pressure is increased and more of the same charged ions become nearest neighbors the liquid Coulomb energy increases considerably. As more of the same charged ions enter the nearest-neighbor shell ΔH continually increases up to 100 kbar. Above this pressure the liquid assumes an inert gaslike structure in which repulsive forces determine the atomic arrangement and the Coulomb terms roughly cancel. As a result further changes in ΔH are small and dT/dP becomes relatively constant.

Analogous pressure-induced changes occur in the solid. It has been reported that solid CsI transforms continuously from a bcc arrangement to a distorted hcp-like structure over the pressure range 0.4 to 1.0 Mbar.[2,3] Atoms in the liquid are less constrained and increasing the pressure and temperature leads to more highly coordinated arrangements at lower pressures than in the solid.

The calculated CsI and xenon melting curves are predicted to cross at 410 kbar and 4280 K. But, the CsI slope is appreciably smaller and therefore the two curves do not con-

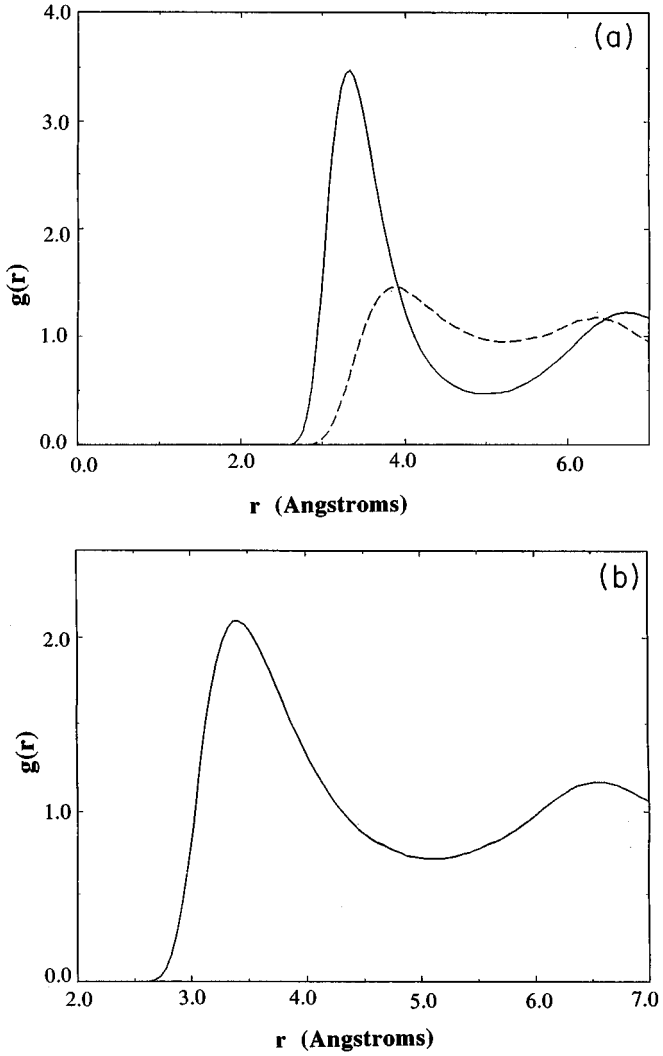

FIG. 10. Radial distribution functions calculated for fluid CsI calculated at 100 kbar and 2700 K. Shown in (a) are the partial functions, $g_{+-}(r)$ and $g_{++}(r)$, as solid and dashed curves, respectively, and in (b) the total $g(r)=[g_{+-}(r)+g_{++}(r)]/2$.

verge. The reason is that, although liquid Xe and CsI have similar atomic orderings, solid CsI retains a large Coulomb energy. Consequently, ΔH of melting is much larger for CsI and its dT/dP is smaller. The value of dT/dP calculated for xenon at 4800 K by molecular dynamics is 6.1 K/kbar, in good agreement with value of 6.2 K/kbar obtained from corresponding states theory. For CsI, the calculated dT/dP is

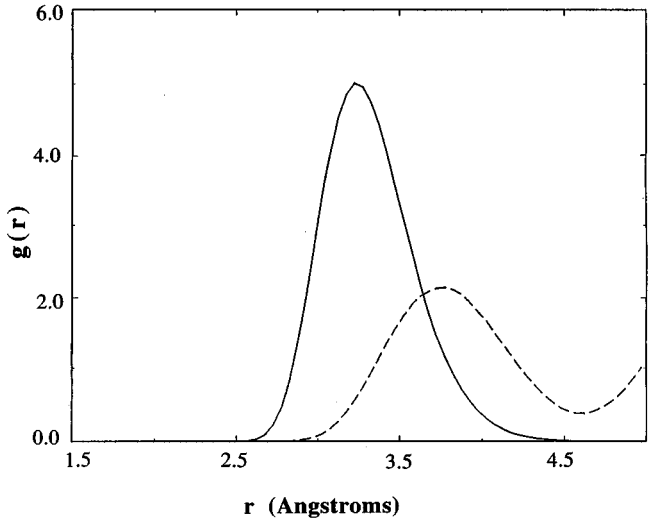

FIG. 11. Radial distribution functions for solid CsI, shown as solid and dashed curves, respectively, calculated near melting at 300 kbar and 3840 K.

3.2 K/kbar. Only a CsI solid without ion-Coulomb energy would lead to a melting slope the same as Xe. This could occur above 1.4 Mbar where both are metallic.

Boness and Brown[13] have suggested that metastability can be the source of the superheating observed in shock experiments. Our results appear to bear them out. Figure 11 shows the radial distribution function of the solid near melting point at 300 kbar, near the shock melting point at 320 kbar. It is seen that the arrangement of ions in the solid differs significantly from the liquid (i.e., Fig. 10), unlike the situation for most monatomic solids. This suggests that the solid is locked in and cannot melt during the several nanosecond time scale available in a shock experiment. This would lead to the observed superheating.[12]

The results reported in this paper are, to our knowledge, the highest temperature static melting measurements made for alkali halides and a method for calculating melting curves by direct integration of the Clapeyron equation.

ACKNOWLEDGMENTS

We wish to thank D. A. Young for many valuable discussions and Bill Hoover for bringing the work of Dr. D. A. Kofke to our attention. The work of D. Boercker and M. Ross was performed under the auspices of the U.S. Department of Energy and by the Lawrence Livermore National Laboratory under Contract No. W-7405-Eng-48.

[1] R. Boehler, Nature (London) **363**, 534 (1993).
[2] H. K. Mao, Y. Wu, R. J. Hemley, L. C. Chen, J. F. Shu, and L. W. Finger, Science **246**, 649 (1989).
[3] H. K. Mao, Y. Wu, R. J. Hemley, L. C. Chen, J. F. Shu, L. W. Finger, and D. E. Cox, Phys. Rev. Lett. **64**, 1749 (1990).
[4] R. Reichlin, M. Ross, S. Martin, and K. A. Goettel, Phys. Rev. Lett. **56**, 2858 (1986).
[5] K. A. Goettel, J. H. Eggert, and I. F. Silvera, Phys. Rev. Lett. **62**, 665 (1989); R. Reichlin, K. E. Brister, A. K. McMahan, M. Ross, S. Martin, Y. K. Vohra, and A. L. Ruoff, *ibid.* **62**, 669 (1989).
[6] D. A. Kofke, J. Chem. Phys. **98**, 4149 (1993).
[7] D. A. Kofke, Mol. Phys. **78**, 1331 (1993).
[8] R. Boehler, N. V. Bargen, and A. Chopelas, J. Geophys. **95**, 21 731 (1990).
[9] C. W. F. T. Pistorious, J. Phys. Chem. Solids, **26**, 1543 (1965).

[10] S. B. Kormer, Sov. Phys. Usp. **11**, 229 (1968).
[11] H. B. Radousky, M. Ross, A. C. Mitchell, and W. J. Nellis, Phys. Rev. B **31**, 1457 (1985).
[12] C. A. Swenson, J. W. Shaner, and J. M. Brown, Phys. Rev. B **34**, 7924 (1986).
[13] D. Boness and J. M. Brown, Phys. Rev. Lett. **71**, 2931 (1993).
[14] L. D. Landau and E. M. Lifshitz, *Statistical Physics* (Pergamon, London, 1958).
[15] S. Nose and F. Yonezawa, J. Chem. Phys. **84**, 1803 (1986).
[16] C-S Zha, R. Boehler, D. A. Young, and M. Ross, J. Chem. Phys. **85**, 1034 (1986).
[17] W. G. Hoover and F. H. Ree, J. Chem. Phys. **49**, 3609 (1968).
[18] W. G. Hoover, M. Ross, K. W. Johnson, D. Henderson, J. A. Barker, and B. C. Brown, J. Chem. Phys. **52**, 4931 (1970).
[19] M. Ross and F. J. Rogers, Phys. Rev. B **31**, 1463 (1985).
[20] M. Dixon and M. J. L. Sangster, J. Phys. C **10**, 3015 (1977).
[21] M. Parrinello and A. Rahman, Phys. Rev. Lett. **45**, 1196 (1985).
[22] M. P. Allen and D. J. Tildesley, *Computer Simulation of Liquids* (Clarendon, Oxford, 1987).
[23] D. B. Boercker, Phys. Rev. B **44**, 11 592 (1991).
[24] S. Ogata and S. Ichimaru, Phys. Rev. A **42**, 4867 (1990).
[25] P. H. Lahr and W. G. Eversole, J. Chem. Eng. Data **7**, 42 (1962).
[26] W. L. Vos, M. G. E. Van Hinsberg, and J. A. Schouten, Phys. Rev. B **42**, 6106 (1990).
[27] W. L. Vos, J. A. Schouten, D. A. Young, and M. Ross, J. Chem. Phys. **94**, 3835 (1991).
[28] T. L. Hill, *Introduction to Statistical Thermodynamics* (Addison-Wesley, Reading, MA, 1960).